engineering proceedings

MDPI

Proceeding Paper

Prototype Wing Design and Manufacturing for Reflexed Airfoil Morphing †

Panagiotis Georgopoulos *,‡, Jurij Sodja and Roeland De Breuker

Aerospace Structures and Materials, Faculty of Aerospace Engineering, Delft University of Technology, 2629 HS Delft, The Netherlands; j.sodja@tudelft.nl (J.S.); r.debreuker@tudelft.nl (R.D.B.)

* Correspondence: p.georgopoulos@tudelft.nl

† Presented at the 15th EASN International Conference, Madrid, Spain, 14–17 October 2025.

‡ Current address: Kluyverweg 1, 2629 HS Delft, The Netherlands.

Abstract

This paper presents the development of a novel morphing wing prototype with three camber-twist morphing flaps. Reflexed airfoil morphing is achieved by means of two chordwise degrees-of-freedom, thereby decoupling lift from the aerodynamic moment with respect to the aerodynamic centre. The prototype wing design is characterised by a novel morphing flap concept and driven by the boundary conditions pertinent to the wind tunnel testing facilities and the choice of research questions. The flaps' spanwise ends are adapted to represent a seamless and a discontinuous transition between adjacent flaps. Linear electric motors induce the morphing shapes, equipped with load cells on their respective push rods, for actuator force measurement. Pressure taps are included to measure the pressure distribution along the wing section. Upon manufacturing, preliminary static test results validate the wing's morphing functionality. The morphing trailing edge demonstrates a range of camber morphing and twist morphing shapes, as well as the ability to support asymmetric morphing between adjacent flaps.

Keywords: morphing flap; camber; twist; reflexed airfoil; prototype wing; wind tunnel testing

1. Introduction

Morphing wings *"change shape in flight in a controlled manner to improve aircraft performance"* [1]. Numerous review papers outline the wide range of developed concepts and morphing modes [1–3]. Among them, camber morphing yields a higher lift-to-drag ratio C_l/C_d relative to a conventional hinged flap, while twist morphing controls the spanwise lift distribution [3]. Such flexible wings were first employed on the Wright Flyer for roll control [2] and have been the focus of multiple research projects since the 1980s in the United States [4–6] and Europe [7,8], among other countries. Over the last decade, small-scale wind tunnel and flight testing has demonstrated C_l/C_d improvements of over 20% [9], high in-flight lift and rolling moments [10] and spanwise aerodynamic load control in the presence of multiple seamlessly connected camber morphing flaps [11]. Full-scale prototypes have also been built and tested in static conditions [12] as well as in-flight [13].

A small subset of studies explore the benefits of multiple morphing degrees of freedom (DoF) along the chord [14,15], including increased control of the morphing flap shape. Small-scale wind tunnel testing has demonstrated the ability to control the moment coefficient around the aerodynamic centre C_{mac} decoupled from the lift coefficient C_l [15]. Ultimately, this augments the camber morphing functionality, to include a family of

Check for updates

Academic Editors: Spiros Pantelakis, Andreas Strohmayer and Gustavo Alonso

Published: 28 April 2026

Copyright: © 2026 by the authors. Licensee MDPI, Basel, Switzerland. This article is an open access article distributed under the terms and conditions of the Creative Commons Attribution (CC BY) license.

shapes, such that for a given value of C_l, there exists a range of attainable C_{mac}, as shown in Figure 1. As opposed to conventional 1-DoF camber morphing, 2-DoF camber morphing is characterised by reflexed airfoil shapes. This functionality yields trim drag reduction by controlling the trim angle of attack and mitigating the required down-lift at the tail.

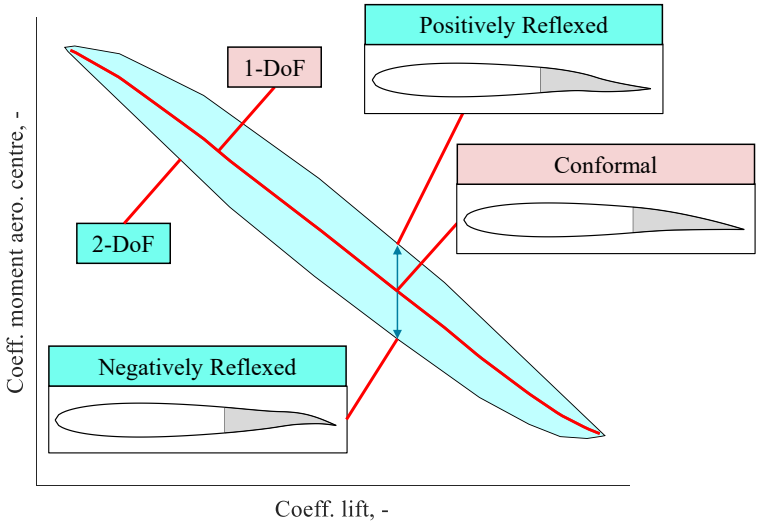


Figure 1. Schematic representation of the 2-DoF camber morphing functionality.

This paper presents the design and manufacturing of a morphing wing prototype, featuring three camber-twist morphing flaps with two chordwise morphing DoF. The prototype was developed for testing in the Low-Speed Tunnel (LST) of the German–Dutch Wind Tunnels (DNW) [16], with the intention of demonstrating the morphing technology at large scale. The poor scalability of morphing wing concepts is identified as a factor delaying the technology's maturation [17]. Indeed, morphing wing wind tunnel testing rarely exceeds $Re = 3 \times 10^6$ [18]. The envisioned experiments will therefore reach a Reynolds number of up to $Re = 4 \times 10^6$, thereby representing the outboard section of a next-generation regional aircraft in low-speed flight [19]. In addition, testing aims to answer the following three research questions:

1. What is the range of attainable C_l and C_{mac} over a range of angles of attack α?
2. How does the optimal C_l/C_d value and shape vary over a range of α?
3. How does drag over the transition region between adjacent morphing flaps compare between a seamless and a discontinuous design?

The remainder of this paper is structured as follows. The morphing flap concept is presented in Section 2. The design and manufacturing of the prototype wing is presented in Section 3. The morphing functionality is then demonstrated in Section 4 with a selection of static morphing shapes. Section 5 summarises the key conclusions drawn.

2. Morphing Flap Concept

The morphing flap concept is depicted in Figure 2. Given the wind tunnel dimensions of 2.25 m × 3 m [16], the flap has a chord length of $c = 0.8$ m and a span length of $l = 0.75$ m, such that three flaps along the axis lead to a wing span of $L = 2.25$ m, matching the height of the test section. The NACA0012 profile was chosen as the baseline shape and the onset of morphing was set to the 60%-chord position.

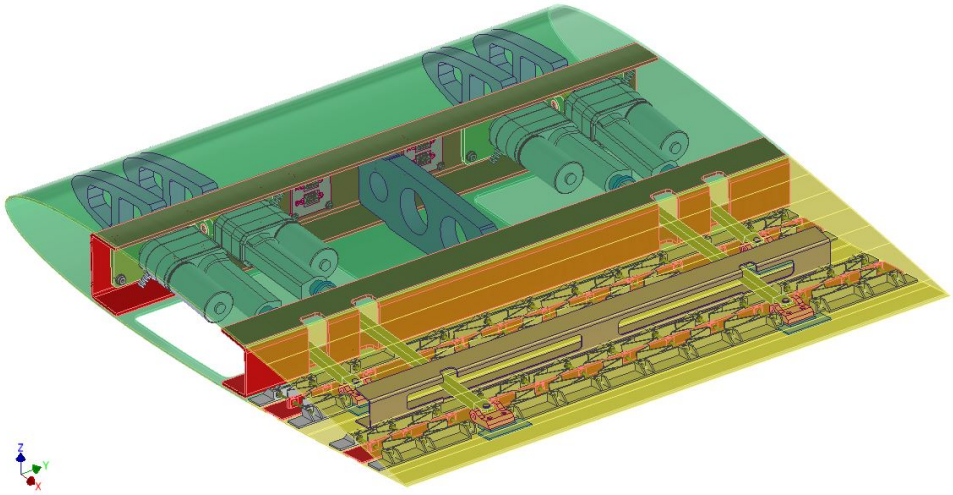


Figure 2. Morphing flap design.

The concept is characterised by the following design features, as shown in Figure 3. The morphing TE skin is made of glass fibre twill fabric oriented at 0°/90° with respect to the span axis. Its stiffness is tailored via chordwise ply-dropping. A pair of spanwise slits is introduced on the pressure-side skin. The skin segmentation is inspired by the TRanslation Induced Camber (TRIC) concept, where a spanwise discontinuity in the pressure-side skin allows chordwise translation of the skin, thereby morphing the trailing edge (TE) [20]. In the presence of two slits, reflexed airfoil morphing is achieved via chordwise translation in opposite directions. The skin on either side of the slits is joined by means of a flexible structure featuring leaf springs and rods, capable of chordwise translation. The structure replaces the stiff guide slot of the TRIC concept, instead matching the skin's bending stiffness and imparting high flexibility in twist. A focused view of the flexible structure concept is included in Figure 3. The depicted segment is repeated along the span. Regarding actuation, a total of four linear electric motors are included per flap. A chordwise pair is needed to achieve reflexed shapes. Two such pairs are needed, one on each spanwise end, to achieve twist. The actuators are connected to the front spar and the pressure-side skin via universal joints. Finally, a trailing edge spar is introduced between the two slits, capable of transmitting the moments necessary to morph into reflexed shapes.

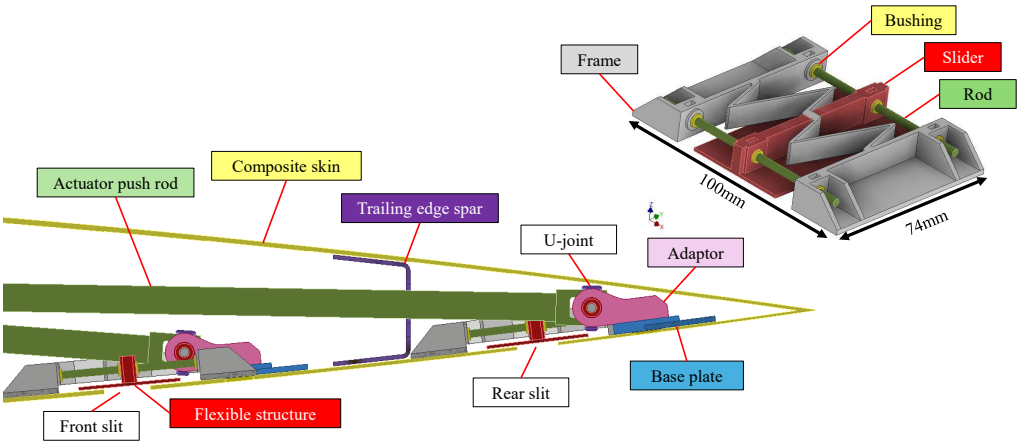


Figure 3. Trailing edge section view focusing on key components, including a focused view of the flexible structure segment.

https://doi.org/10.3390/engproc2026133059

3. Prototype Wing Design and Manufacturing

The prototype was developed for wind tunnel testing in the LST, with the intention of demonstrating the morphing technology at large scale and answering the three research questions mentioned in Section 1.

To answer the first two questions, the wing will be morphed into a wide range of camber morphing shapes and tested over a range of angles of attack. Infinite wing conditions require a constant shape along the span;, therefore, mitigating aeroelastic deflections is key. Onboard sensors must be integrated to collect the desired dataset. The measurement of C_l and C_{mac} requires pressure taps near the midspan. Furthermore, the range of $C_l - C_{mac}$ is determined by actuator stroke and force limits; hence, load cells are required to measure the latter. These onboard sensors must be accounted for in the design, as well as cable and tube routing to the exterior. Conversely, drag and morphing shape are measured via external sensing systems, specifically with a pitot rake and 3D marker-tracking system.

The answer to the third question can be found in the wake velocity deficit aft of the transition region between adjacent flaps, to be measured with the pitot rake in the presence of asymmetric morphing between adjacent flaps. The spanwise ends of the flaps must therefore be adapted to recreate a seamless transition between Flaps 1 and 2 and a discontinuous transition between Flaps 2 and 3. The two subsystems are labelled as Transition Region—Seamless (TRS) and Transition Region—Discontinuous (TRD).

Given the above considerations, a morphing wing design is obtained, as shown in Figure 4. Starting with the wingbox, a high-stiffness structure was necessary to mitigate aeroelastic deflections in the presence of aerodynamic loads. Hence, the skin was made of carbon fibre reinforced laminate, enclosing two steel spars, as well as a steel interface on both spanwise ends to allow clamping to the tunnel. Steel ribs help resist the actuator loads acting on the front spar web. Access hatches are included on the pressure-side skin, allowing interior access for repairs.

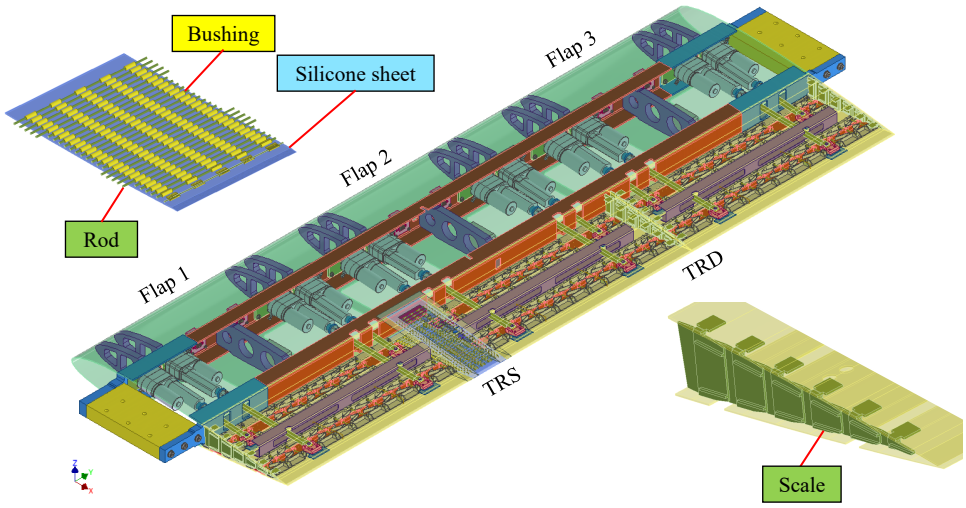


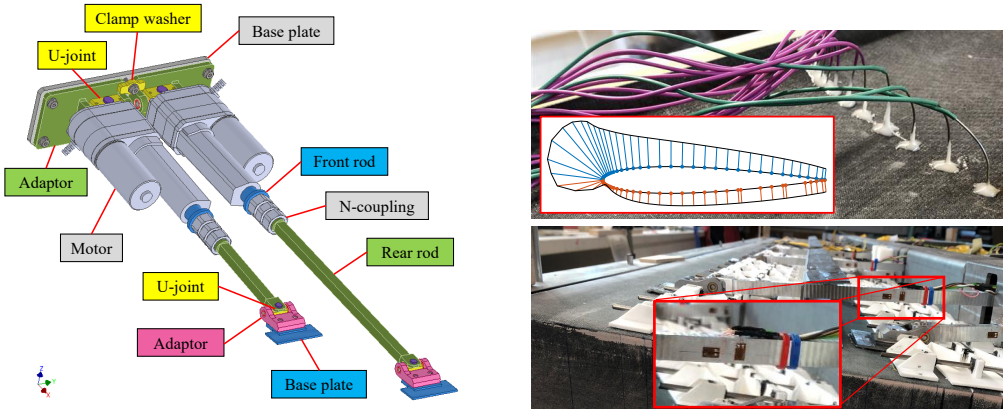
Figure 4. Prototype wing design focusing on TRS and TRD design.

In the TE, the two flap transition designs are shown. The TRS connects Flaps 1 and 2 seamlessly by means of a 80 mm wide silicone skin, reinforced with spanwise steel rods for bubbling mitigation, supported by bushings joined to the skin. The structure has high in-plane flexibility, allowing asymmetric morphing between the two flaps. Conversely, Flaps 2 and 3 are disconnected. The TRD features scales joined to the suction-side skin, mitigating air flow to the flap interior.

Onboard instrumentation includes actuators and sensors, as shown in Figure 5. A pair of actuators is presented in Figure 5a. The DSZY1-24-40-050-POT-IP65 linear electric motor

provides ±1000 N force, 50 mm stroke, a non-backdriveable gearbox, and an integrated potentiometer for stroke control [21]. The actuators are joined to the front spar web and the pressure-side skin with custom-made universal joints connected to adaptors, which are bolted to base plates. Given the high forces and small dimensions required, these components are made from steel. The actuator push rod is made of two rods connected axially via N-coupling. The N-coupling can be loosened through the access hatch, allowing the actuators to be removed from the wing interior for repairs.

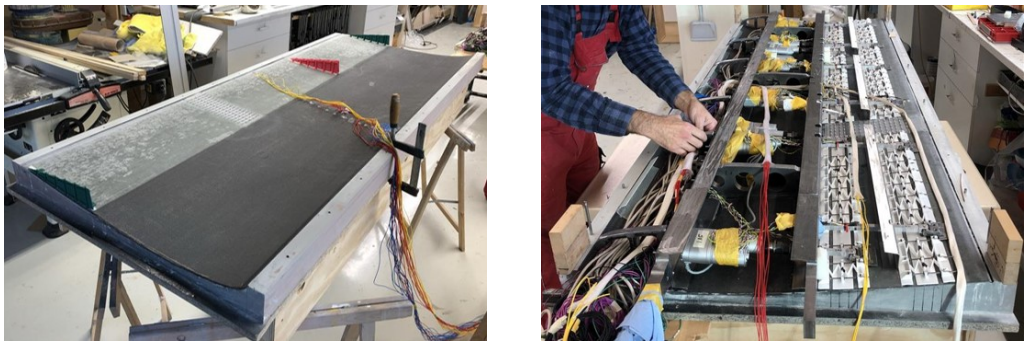
Each actuator push rod is equipped with a load cell, as shown in Figure 5b. The load cells measure axial force using four strain gauges in the type III full-bridge configuration, mitigating the signal due to bending strain and temperature variation. The rear rod is made of high-strength aluminium as opposed to steel, leveraging the lower Young's modulus to improve the signal-to-noise ratio. Finally, a total of 68 pressure taps are included at the midspan, as shown schematically in Figure 5b. The cables and tubes are routed to the exterior along the hollow D-nose.



(**a**) (**b**)

Figure 5. Onboard instrumentation. (**a**) Actuator assembly. (**b**) Pressure taps and load cells.

The prototype prior to assembly is shown in Figure 6. First, the composite skin was manufactured, by vacuum curing the wet-laid glass fibre and carbon fibre in polyurethane moulds. The two fabric types were staggered over a region below the rear spar flanges. The silicone skin of the TRS was included with the laminate to ensure adhesion to the skin upon curing. The bushings and rods of the TRS were installed after curing. As seen in Figure 6b, most components were installed on the pressure-side skin, with the exception of the TRD scales. The two halves were joined with epoxy resin along the leading and trailing edge.



(**a**) (**b**)

Figure 6. Prototype wing manufacturing. (**a**) Suction-side assembly. (**b**) Pressure-side assembly.

4. Morphing Functionality Validation

This section presents a selection of morphing shapes to demonstrate the prototype's functionality. The shapes were measured using markers on the suction-side skin.

The flap's ability to morph in a wide range of conformal camber morphing shapes is presented in Figure 7. The morphing shapes are presented relative to the unmorphed NACA0012 profile. An equivalent flap deflection angle θ is defined between the x-axis and the line segment connecting the $\{x = 0.48$ m$, z = 0$ m$\}$ point and the TE tip. The shapes range from $\theta = -5.50°$ to $\theta = 10.79°$. The colour of each shape corresponds to its θ value. Morphing in the negative θ direction is limited by localised skin bulging at the load application point by the rear actuator push rods.

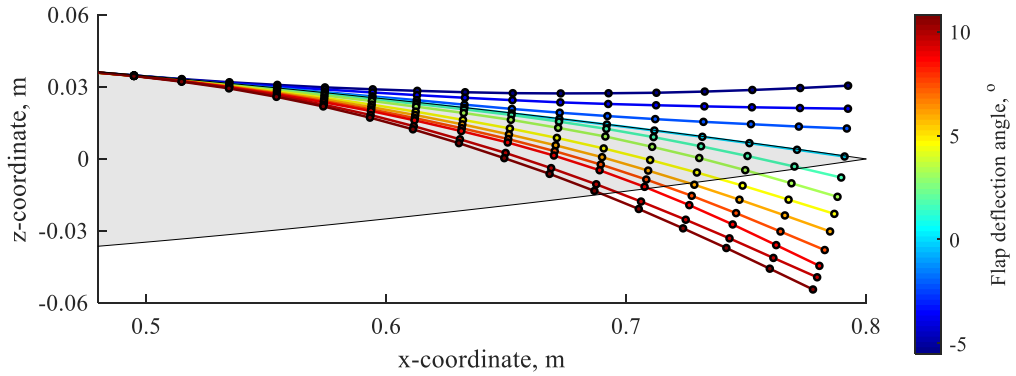


Figure 7. Conformal morphing shapes.

The reflexed airfoil morphing functionality is shown in Figure 8. The graphs show the evolution of the shapes as they transition from a high-C_l shape, in red, to a low-C_l shape, in blue. The characteristic curvature associated with reflexed airfoils can be observed. The curvature is more pronounced in the low-C_l shapes. This would lead to a higher range of C_{mac} values for a low value of C_l compared to for a high value of C_l, as anticipated.

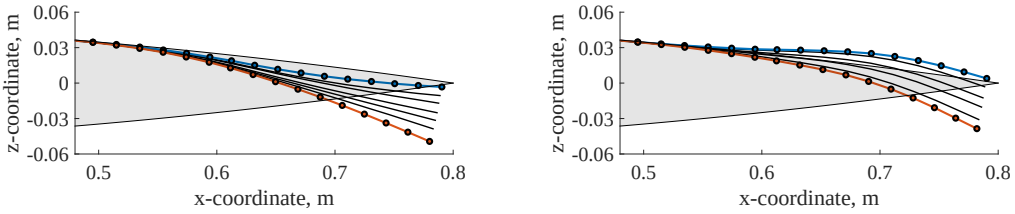


Figure 8. Reflexed morphing shapes. (**a**) Positively reflexed. (**b**) Negatively reflexed.

The ability of the TRS to support asymmetric camber morphing is shown in Figure 9, using the position of the markers along the TE tip. Actuator strokes on Flap 2 were kept fixed while gradually morphing Flap 1. Using the previous definition of θ, the difference in flap deflection angle between the two flaps $\Delta\theta$ is calculated. The TRS was found to support asymmetric morphing up to $\Delta\theta = 6.78°$.

Finally, the wing's twist morphing ability is presented in Figure 10. The flaps are morphed in twist, thereby maintaining a continuous, straight TE across flaps. This ability is vital, especially in the case of the TRD design, to minimise the wake velocity deficit. A twist angle ϕ is defined between the y-axis and the line formed by the markers along the TE tip. The wing exhibits twist morphing up to $\phi = 1.67°$. It is noted that individual flaps can twist beyond this value. However, the requirement for a straight, continuous TE causes the spanwise ends of the wing to approach the limits of attainable θ.

https://doi.org/10.3390/engproc2026133059

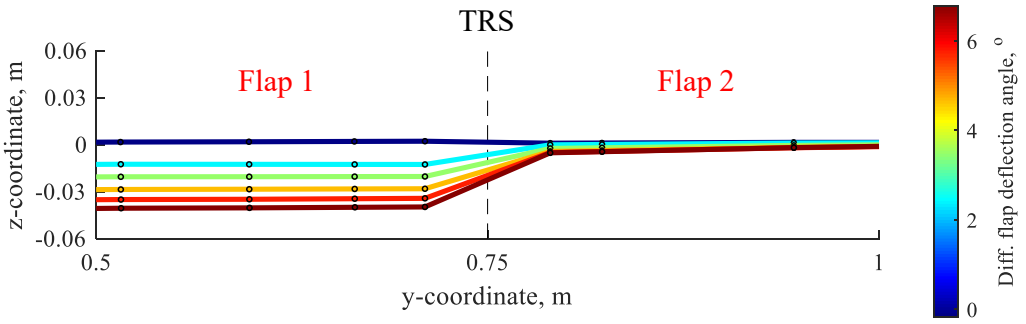


Figure 9. Asymmetric camber morphing between adjacent flaps.

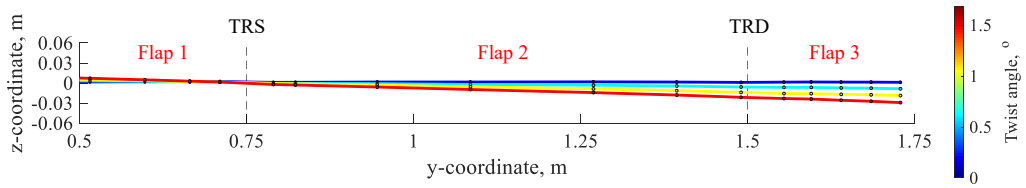


Figure 10. Twist morphing across the wing's trailing edge.

5. Conclusions

This paper presents the development of a prototype wing featuring three novel camber-twist morphing flaps capable of reflexed airfoil morphing. The design is driven by the boundary conditions imposed by the LST facilities and the choice of research questions.

At the flap level, a selection of components combine to impart the novel morphing functionality. These include two spanwise slits on the pressure-side skin, chordwise flexible structures joining the discontinuous skin, four linear actuators, and a trailing edge spar. The flaps are integrated with a high-stiffness wingbox, characterised by carbon fibre skin and steel spars. The wingbox mitigates aeroelastic deflections, thereby promoting infinite wing conditions. In addition, a seamless transition between Flaps 1 and 2 is achieved using a silicone skin structure, reinforced with steel rods. Conversely, Flaps 2 and 3 are disconnected, to compare the influence of the two designs. The wing is actuated by a total of 12 commercially available linear electric motors featuring load cells on each push rod, in the form of four strain gauges in the type III full-bridge configuration. The pressure distribution along the wing section is measured using 68 pressure taps at midspan.

Upon manufacturing, the envisioned morphing functionality was demonstrated. A wide range of conformal camber morphing shapes was achieved, from $\theta = -5.50°$ to $\theta = 10.79°$. Positively and negatively reflexed morphing shapes were also obtained, exhibiting more pronounced curavtures at low-C_l shapes. The TRS demonstrated the ability to support a high degree of asymmetric morphing between adjacent flaps, up to $\Delta\theta = 6.78°$. Finally, the wing is capable of maintaining a straight, continuous TE across flaps, by twisting the three flaps accordingly up to $\phi = 1.67°$.

Supplementary Materials: The following supporting information can be downloaded at: https://www.mdpi.com/article/10.3390/engproc2026133059/s1.

Author Contributions: Conceptualisation, P.G., J.S. and R.D.B.; methodology, P.G.; software, P.G.; validation, P.G.; formal analysis, P.G.; investigation, P.G.; resources, P.G., J.S. and R.D.B.; data curation, P.G.; writing—original draft preparation, P.G.; writing—review and editing, J.S. and R.D.B.; visualisation, P.G.; supervision, J.S. and R.D.B.; project administration, R.D.B.; funding acquisition, R.D.B. All authors have read and agreed to the published version of the manuscript.

Funding: The authors acknowledge the financial support of the Dutch government through the Netherlands Enterprise Agency (RVO) under the TSH Vliegtuigmaakindustrie programme, project number TSH21009. The RICHTING project (Radicale weerstands en gewICHTsreductie door morphING en microstructuren) started on 1 January 2022 and ended on 30 June 2025.

Data Availability Statement: The original contributions presented in this study are included in the supplementary material. Further inquiries can be directed to the corresponding author.

Acknowledgments: The authors acknowledge the partnering organisations from the RICHTING project: Dutch-German Wind Tunnels (DNW), Royal Netherlands Aerospace Laboratory (NLR), Qlayers, Netherlands Organisation for Applied Scientific Research (TNO). In addition, the authors acknowledge Wouter Gregoor and Hans van der Does at DEMO (Dienst Elektronische en Mechanische Ontwikkeling) in Delft, The Netherlands, for their respective support in the design of the wing and the development of the actuator control instrumentation. Finally, the authors acknowledge Martin Weberschock at Weberschock Development in Gleichen, Germany, for manufacturing the wing.

Conflicts of Interest: The authors declare no conflicts of interest.

References

1. Vasista, S.; Tong, L.; Wong, K.C. Realization of Morphing Wings: A Multidisciplinary Challenge. *J. Aircr.* **2012**, *49*, 11–28. [CrossRef]
2. Weisshaar, T.A. Morphing Aircraft Systems: Historical Perspectives and Future Challenges. *J. Aircr.* **2013**, *50*, 337–353. [CrossRef]
3. Harvey, C.; Gamble, L.L.; Bolander, C.R.; Hunsaker, D.F.; Joo, J.J.; Inman, D.J. A review of avian-inspired morphing for UAV flight control. *Prog. Aerosp. Sci.* **2022**, *132*, 100825. [CrossRef]
4. Perry, B.; Cole, S.R.; Miller, G.D. Summary of an Active Flexible Wing program. *J. Aircr.* **1995**, *32*, 10–15. [CrossRef] [PubMed]
5. Sanders, B.; Crowe, R.; Garcia, E. Defense Advanced Research Projects Agency—Smart Materials and Structures Demonstration Program Overview. *J. Intell. Mater. Syst. Struct.* **2004**, *15*, 227–233. [CrossRef]
6. McGowan, A.M.R.; Washburn, A.E.; Horta, L.G.; Bryant, R.G.; Cox, D.E.; Siochi, E.J.; Padula, S.L.; Holloway, N.M. Recent results from NASA's morphing project. In *Proceedings of the Smart Structures and Materials 2002: Industrial and Commercial Applications of Smart Structures Technologies*; International Society for Optics and Photonics, SPIE: San Diego, CA, USA, 2002; Volume 4698, pp. 97–111. [CrossRef]
7. De Gaspari, A.; Ricci, S.; Antunes, A.; Odaguil, F.; Rodrigues de Lima, G. Application of Active Camber Morphing Concept to a Regional Aircraft. In Proceedings of the 22nd AIAA/ASME/AHS Adaptive Structures Conference 2014, National Harbor, MD, USA, 13–17 January 2014. [CrossRef]
8. Wölcken, P.C.; Papadopoulos, M. *Smart Intelligent Aircraft Structures (SARISTU): Proceedings of the Final Project Conference*; Springer: Cham, Switzerland, 2016. [CrossRef]
9. Woods, B.K.S.; Bilgen, O.; Friswell, M.I. Wind tunnel testing of the Fish Bone Active Camber morphing concept. *J. Intell. Mater. Syst. Struct.* **2014**, *25*, 772–785. [CrossRef]
10. Molinari, G.; Arrieta, A.F.; Ermanni, P. Planform, aero-structural and flight control optimization for tailless morphing aircraft. *J. Intell. Mater. Syst. Struct.* **2018**, *29*, 3847–3872. [CrossRef]
11. Nguyen, N.; Lebofsky, S.; Ting, E.; Kaul, U.; Chaparro, D.; Urnes, J. Development of Variable Camber Continuous Trailing Edge Flap for Performance Adaptive Aeroelastic Wing. In *Proceedings of the SAE 2015 AeroTech Congress & Exhibition*; SAE International: Seattle, WA, USA, 2015. [CrossRef]
12. Pecora, R. Morphing wing flaps for large civil aircraft: Evolution of a smart technology across the Clean Sky program. *Chin. J. Aeronaut.* **2021**, *34*, 13–28. [CrossRef]
13. Kota, S.; Flick, P.; Collier, F.S. Flight Testing of FlexFloil Adaptive Compliant Trailing Edge. In Proceedings of the 54th AIAA Aerospace Sciences Meeting, San Diego, CA, USA, 4–8 January 2016. [CrossRef]
14. Pankonien, A.M.; Faria, C.T.; Inman, D.J. Synergistic smart morphing aileron: Experimental quasi-static performance characterization. *J. Intell. Mater. Syst. Struct.* **2015**, *26*, 1179–1190. [CrossRef]
15. Wu, R.; Soutis, C.; Zhong, S.; Filippone, A. A morphing aerofoil with highly controllable aerodynamic performance. *Aeronaut. J.* **2017**, *121*, 54–72. [CrossRef]
16. Low-Speed Tunnel. Available online: https://www.dnw.aero/wind-tunnels/lst/ (accessed on 5 November 2025).
17. Ameduri, S.; Concilio, A. Morphing wings review: Aims, challenges, and current open issues of a technology. *Proc. Inst. Mech. Eng. Part C J. Mech. Eng. Sci.* **2020**, 237, 4112–4130. [CrossRef]
18. Majid, T.; Jo, B.W. Status and Challenges on Design and Implementation of Camber Morphing Mechanisms. *Int. J. Aerosp. Eng.* **2021**, *2021*, 6399937. [CrossRef]

19. Eberle, A.; Stefes, B.; Reckzeh, D. Clean Aviation Ultra-Performance Wing (UP-Wing). In Proceedings of the AIAA SCITECH 2024 Forum, Orlando, FL, USA, 8–12 January 2024. [CrossRef]
20. Mkhoyan, T.; Thakrar, N.R.; De Breuker, R.; Sodja, J. Morphing wing design using integrated and distributed trailing edge morphing. *Smart Mater. Struct.* **2022**, *31*, 125025. [CrossRef]
21. Elektrozylinder DSZY1-POT (Mit Potentiometer). Available online: https://www.msw-motion.de/produkt/dszy1-pot/ (accessed on 5 November 2025).

Disclaimer/Publisher's Note: The statements, opinions and data contained in all publications are solely those of the individual author(s) and contributor(s) and not of MDPI and/or the editor(s). MDPI and/or the editor(s) disclaim responsibility for any injury to people or property resulting from any ideas, methods, instructions or products referred to in the content.